Nonlinear longitudinal dynamics studies at the ALS *

J. M. Byrd†, W-H Cheng, S. DeSantis, D. Li, LBNL, G. Stupakov, F. Zimmermann, SLAC

Abstract

We present a summary of results for a variety of studies of nonlinear longitudinal dynamics in the Advanced Light Source, an electron storage ring. These include observation of decoherence at injection, decay of an injected beam, forced synchrotron oscillations and diffusion from one bunch to the next. All of the measurements were made using a dual–scan streak camera which allowed the real-time observation of the longitudinal distribution of the electron beam.

Introduction Synchrotron oscillations are inherently nonlinear, mostly because of the sinusoidal radiofrequency (RF) voltage used to longitudinally focus the beam. When the bunch length is small compared to the RF wavelength, the RF voltage over the length of the bunch can be considered as linear, minimizing nonlinear effects. In electron storage rings, this is almost always the case. However, as the performance demands on electron rings grow, it becomes increasingly important to understand several of the subtle effects caused by the nonlinearities. These effects are also fascinating unto themselves and their study constitutes a contribution to the physics of beams. This paper presents a summary of results of experimental studies of several nonlinear effects in longitudinal beam dynamics in the Advanced Light Source (ALS), an electron storage ring optimized for producing high brightness synchrotron radiation. Machine parameters relevant to our experiments are listed in Table 1. Due to space considerations, only a qualitative description of the results are presented here. More theoretical and experimental details can be found elsewhere[2, 5, 6].

Section II describes the streak camera used for all of the results in this paper. Section III presents a study of injection transients with and without beam capture. Section IV presents measurements of diffusion from one bunch to another. Section V describes measurements of forced nonlinear synchrotron oscillations. Section VI summarizes the paper.

Dual scan streak camera To make a detailed study of the longitudinal beam dynamics, we used a streak camera (SC) to observe the evolution of the longitudinal bunch distribution. A schematic diagram of the Hamamatsu C5680 SC is shown in Figure 1. The SC converts the time structure of a pulse of synchrotron radiation at optical wavelengths from a bend magnet into vertical deflection at the CCD camera. In our experiments, the vertical deflection plates are driven by a 125 MHz sinusoidal voltage synchronized to the RF frequency. In addition, there is an optional slow horizontal deflection which allows observation of the longitudinal profile as a function of time. The time scale of the horizontal sweep can be adjusted to observe several turns or thousands of turns and can be triggered to coincide with an event such as injection. For sweep times longer than several hundred turns, individual turns can no longer be resolved and so the longitudinal profile appears as a continuous line across the image.

The synchroscan principle is illustrated in Fig. 2 which shows the 125 MHz vertical deflecting voltage with respect to the arrival times of 4 storage ring bunches. Only deflections within the marked bands appear on the microchannel, allowing an effective means of gating a particular bunch. The phase of the deflecting voltage can be adjusted to place the arrival of a single bunch on the center of the screen.

Parameter	Description	Value
E	Beam energy	1.5 GeV
C	Circumference	196.8 m
f_{rf}	RF frequency	499.664 MHz
V_{rf}	RF voltage	1.1 MV
h	Harmonic number	328
α	Momentum compaction	1.6×10^{-3}
Q_s	Synchrotron tune	0.0075
λ_{rad}	Long. rad. damping rate	5×10^{-5}
σ_ℓ	RMS natural bunch length	4.5 mm
σ_ϵ	RMS $\delta E/E$	7.1×10^{-4}

Table 1: Nominal ALS longitudinal parameters.

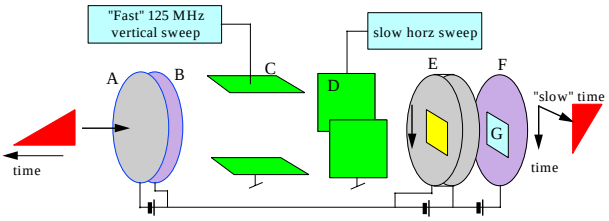

Figure 1: Schematic diagram of the streak camera in synchroscan mode with dual sweep. A: photocathode, B: accel. mesh, C: vert. deflection electrode, D: horz. defl. electrode, E: microchannel plate F: phosphor screen, G: CCD camera.

* This work was supported by the U.S. Dept. of Energy under Contract Nos. DE-AC03-76SF00098 and DE-AC03-76SF00515.

† JMByrd@lbl.gov

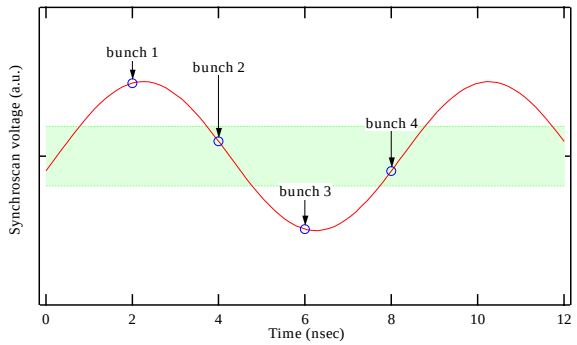

Figure 2: Vertical deflecting voltage shown with respect to the arrival times of 4 storage ring bunches. Only deflections within the marked bands are observed.

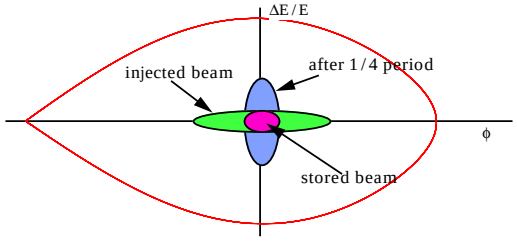

Figure 3: Illustration of quadrupole bunch oscillations at injection for bunch mismatched to the storage ring RF bucket.

Injection transients Optimizing the beam injection into electron rings is important for increasing the filling rate and reducing radiation backgrounds. Understanding the injection process and subsequent transient is particularly important in damping rings for linear colliders and also for continuous injection (i.e. top–up.) This section describes measurements of the longitudinal beam distribution following injection in the ALS.

When an electron bunch is injected into the storage ring, it's length and energy spread will either grow or damp to the natural bunch length and energy spread of the storage ring over several radiation damping times[1]. In the ALS, the injected bunch length is about five times the natural bunch length and the injected energy spread is close to the natural energy spread. If this mismatched bunch is injected into the center of an RF bucket, it rotates in the bucket at the synchrotron frequency, modulating the bunch length as shown schematically in Fig. 3. However, the nonlinearity of the RF voltage creates a dependence of synchrotron frequency on amplitude, causing the bunch head and tail to advance slower in phase than the bunch center, causing a filamentation of the bunch distribution as shown in the results of a computer simulation in Fig. 4.

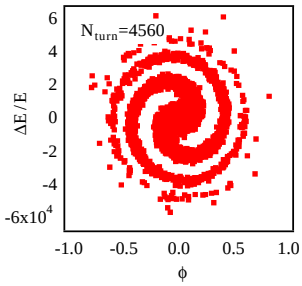

Figure 4: Phase space distribution 4560 turns following injection for ALS injected beam conditions illustrating phase space filamentation.

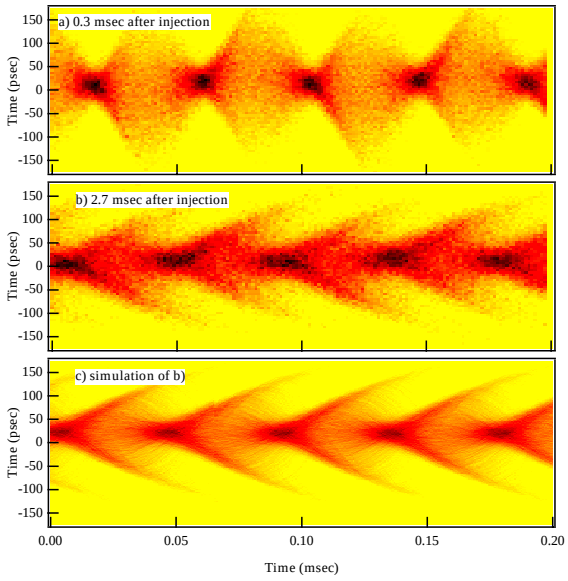

Figure 5: a) Measured SC image 0.3 msec following injection showing modulation of the bunch length. b) SC image 2.4 msec later showing filamentation of the large amplitude particles. c) A computer simulated image found from tracking.

Shown in Fig. 5a is a SC image of beam 0.3 msec following injection into an empty storage ring. The vertical axis represents the longitudinal bunch length in units of time and the horizontal axis is time. The bunch length is modulated at half the synchrotron period of 87 μsec due to the rotation of the mismatched bunch shape as shown in Fig. 3. Fig. 5b shows the SC image 2.4 msec later. The bunch filamentation is evidenced by the tails forming on the bunch distribution. This compares very well with a simulated SC image as shown in Fig. 5c, where each vertical slice is the projection of the phase space distribution as shown in Fig. 4 onto the phase axis.

It is also interesting to examine the decay of an injected beam without RF capture (i.e. no RF voltage). As the beam loses energy, its orbit spirals inwards and

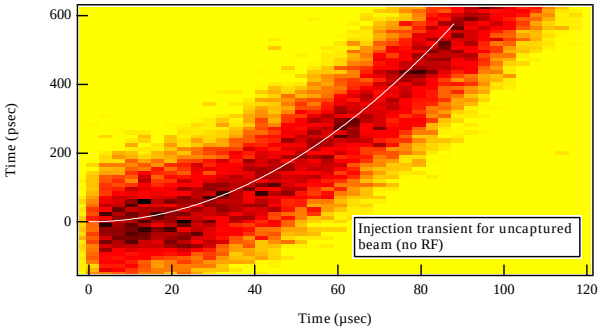

Figure 6: Transient of a decaying, uncaptured electron beam at injection. The calculated drift for parameters given in Table 1 is shown as a white line.

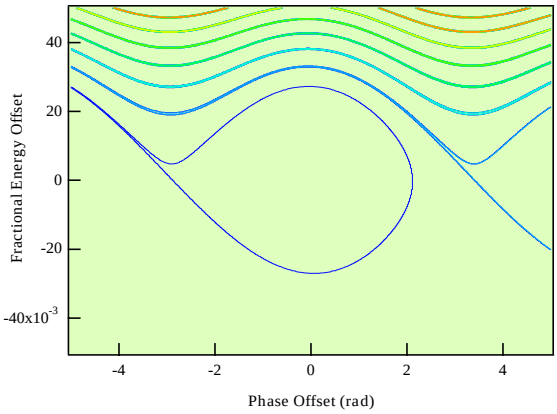

Figure 7: Phase space orbits including radiation damping. The RF buckets are no longer closed, with attractors for following buckets lying above each bucket.

it eventually is lost. The ring orbit period also decreases according to the relation

$$\frac{\Delta T}{T_0} = \alpha \delta_{tot} \tag{1}$$

where α is the momentum compaction, and δ_{tot} is the total frequency energy lost. Assuming the energy loss per turn is constant and α is independent of energy, the path difference is given by

$$\delta_{tot} = \frac{f_0^2 \delta_{turn}}{2} t^2 \tag{2}$$

If the energy loss/turn is known, this may be another technique for measuring the momentum compaction.

Fig. 6 shows a SC image at injection with the storage ring RF turned off. As the uncaptured beam decays, it arrives earlier on each turn w.r.t the synchroscan voltage shown in Fig. 2, creating an increasing vertical deflection on the SC. Also shown is the calculated decrease in orbit period using parameters given in Table 1. We are currently analysing the evolution of the bunch shape.

Bunch-bunch diffusion Ignoring radiation damping, which acts as a frictional damping to the synchrotron oscillations, synchrotron oscillations within the RF bucket are stable. Electrons with synchrotron orbits outside of the RF bucket slowly lose energy and eventually are lost. Generally, this approximation is good because radiation damping times in electron storage rings are typically small compared with synchrotron periods. However, radiation damping provides a mechanism by which electrons with synchrotron orbits outside the RF bucket have a small probability of being recaptured into a subsequent RF bucket. Given an electron bunch stored in a ring, electrons can be ejected from the RF bucket by processes such as large–angle intrabeam (Touschek) scattering or quantum excitation. We refer to the recapture of a fraction of the ejected electrons as a diffusion process. This section presents a brief description and measurements of this diffusion process at the ALS. More details are given elsewhere[2]. Similar studies have been done at UVSOR and the Photon Factory[3].

Although the diffusion process is interesting from the point of view of accelerator physics, it can also be important for operation of a synchrotron light source. For example, one operational mode at several facilities requires large single light pulses separated by at least several hundred nanoseconds to accommodate the time–of–flight techniques used by experimenters. In this mode at the ALS, the ring is filled with two electron bunches separated by 328 nsec. The storage ring injection process typically fills several unwanted parasite bunches which are removed prior to an experiment using a common RF knockout technique. However, the diffusion process can create additional parasite bunches over time, possibly contaminating the experiment.

The effect of the radiation damping on longitudinal phase space is illustrated in Fig. 7. The RF bucket is no longer a closed area but rather a basin of attraction for electrons within the boundaries shown. For a given bucket, the attractors of subsequent buckets lie above the bucket. Electrons ejected from the bucket have a small probability of landing on an attractor and damping to a subsequent bucket. The diffusion rate can be calculated as the product of the the probablity of exciting an electron to an amplitude and the width and position of the attractor. Note the the process is not symmetric in that only particles ejected with too much energy can be recaptured. Also note that other particle loss mechanisms are ignored.

Our experiment consisted of filling a single bunch to a level of several milliamps and recording its current and that of the following parasite bunch as a function of time. The relative current in the parasite bunch was measured using the SC simply as a means of gating the synchrotron light signal such that it could be measured independently from the main bunch.

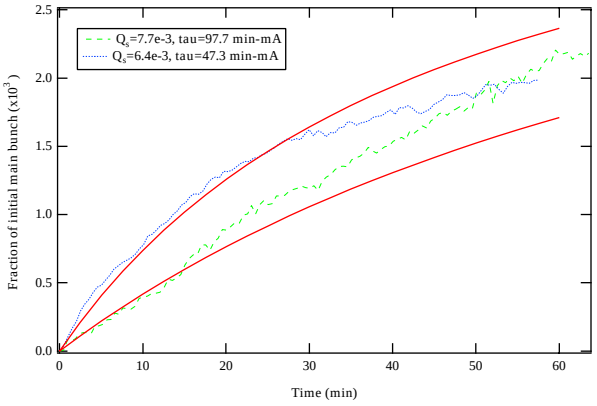

Figure 8: Measured charge in the parasite bunch relative to the main bunch for 2 different RF voltages. The solid lines for each data set are the calculated diffusion using the measured Touschek lifetime for each RF voltage.

Measurement of the diffusion into the parasite bunch relative to the initial charge in main as a function of time is shown in Figure 8. The two cases are for RF voltages of 1.1 and 0.78 MV with corresponding synchrotron tunes of 7.7e-3 and 6.4e-3. Diffusion is faster for lower RF voltages since the attractors are closer to the bunch.

One technique for eliminating the diffusion is to adjust the momentum acceptance of the lattice to be approximately equal to the RF acceptance such that any particle ejected from the bucket is lost. This already occurs in the ALS in some conditions, albeit unintentionally. Studies[4] indicate that the ring momentum acceptance decreases below the RF acceptance when the wiggler is in its fully closed position. We no longer observed the diffusion in this condition.

Forced oscillations The subject of forced, or driven, synchrotron oscillations has many applications in the physics of beams[5]. Forced synchrotron oscillations occur when the beam is driven by modulations of the bending fields or voltage or phase modulations in the RF system. Both of these effects can have significant impact on operation, particularly in efforts to achieve very short electron bunches. This section presents highlights from our studies of phase modulation of synchrotron oscillations. More details are given elsewhere[6].

Synchrotron oscillations are very similar to those of a pendulum, which has a response curve as shown in Fig. 9. When the frequency of the driving force is below the bifurcation frequency, the response has two stable points as also shown in a Poincarè map of the phase space in a frame rotating at the driving frequency. The beam can be distributed between the two islands. If the excitation frequency is swept through the bifurcation point, the actual distribution depends on the initial beam distribution as well as the beam

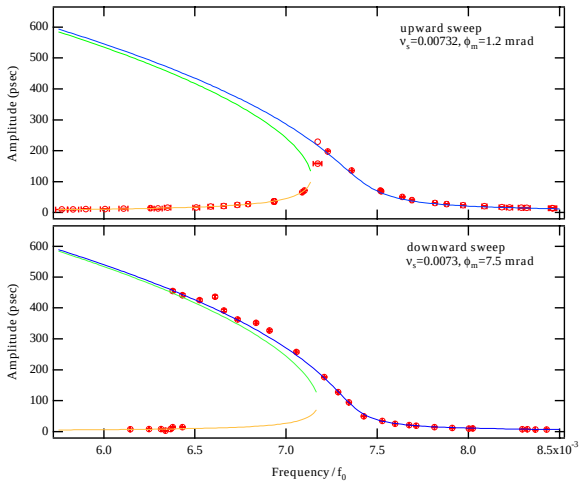

Figure 9: Measured response curve for a modulation frequency swept upwards and downwards through the resonance.

current. Our experiments consisted of mapping the fixed points of the system as a function of modulation amplitude and frequency. We also studied the diffusion process from one island to another and related it to the Touschek scattering process.

An example SC image at a condition where the phase modulation frequency is just below the bifurcation frequency is shown in Fig. 11. As the modulation frequency is swept upwards above the bifurcation frequency, the smaller amplitude island disappears as can be seen from the response curve in Fig. 9. The measured fixed points of the system for a upward and downward sweep of the modulation frequency are shown in Fig. 9. The hysteresis typical of such as system is also evident in the difference between the direction of the swept frequency.

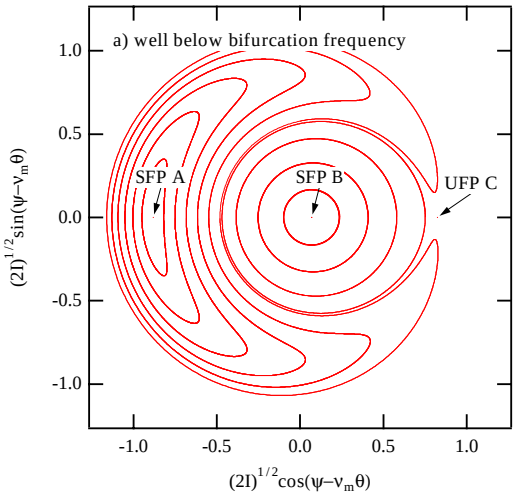

Figure 10: Poincarè map of the phase space in a frame rotating with the modulation frequency when exciting below the below bifurcation frequency.

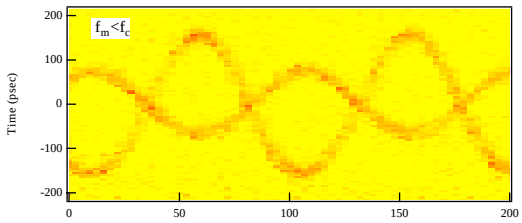

Figure 11: SC Image of the longitudinal profile when the modulation frequency is just below the bifurcation frequency. The beam populates both stable phase space islands.

To measure the interisland diffusion rates, we filled a single bunch with current and used the SC to measure the longitudinal profile as a function of time after initiating the phase modulation at a fixed frequency. The modulation frequency was always below the bifurcation frequency, ensuring the presence of two stable islands. For each beam current, we measured the diffusion as a function of modulation frequency in order to vary the island size and separation.

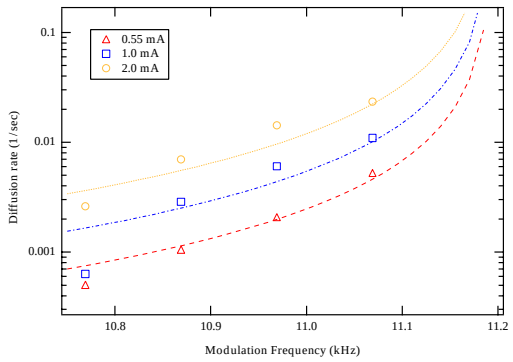

Figure 12: Measured and predicted diffusion rates as a function of modulation frequency for three bunch currents.

We extracted the initial diffusion rate by comparing the relative rate of increase of the peak signal in the island A (outer island) compared to the island B (central island.) A plot of the diffusion rates as a function of modulation frequency for several beam currents is shown in Figure 12. Calculations of the diffusion rate with Touschek scattering as the diffusion mechanism and the separatrix of island B as the momentum acceptance show approximate agreement with the measurements.

We have also studied the structure of higher resonances at multiples of the synchrotron frequency. At twice the synchrotron frequency, two or three phase space islands are expected to form, depending on the modulation frequency. An example is shown in Fig. 13, which shows the bunch split into two islands. The calculated phase space structure is also shown. At three

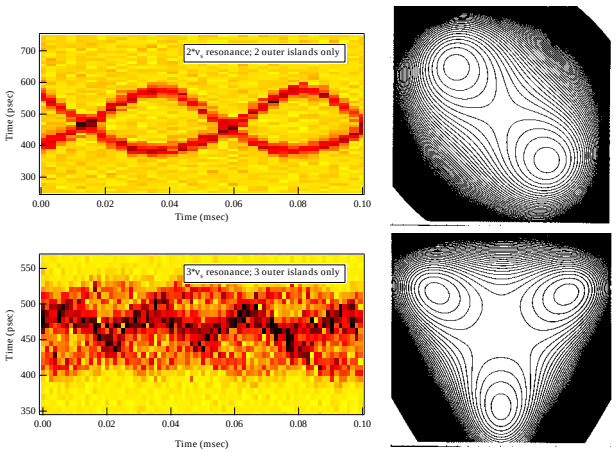

Figure 13: Measured SC image showing formation of two and three islands for excitation near 2^*f_s and 3^*f_s. The calculated phase space structure is also shown.

times the synchrotron frequency three or four islands can form. An example of this resonance is also shown in Fig. 13.

Conclusions The nonlinearity of synchrotron oscillations creates several interesting and subtle effects in electron storage rings. These experiments also demonstrate that the dual–scan SC is an invaluable tool for understanding longitudinal beam dynamics in electron storage rings.

The author would like to thank Dr. Albert Hofman and Prof. S. Y. Lee for many useful discussions on longitudinal dynamics and Dr. Alex Lumpkin, Jim Hinkson, and Mike Chin for helping set up and understand the streak camera.

1 REFERENCES

[1] H. Mosshammer, Phys. Rev. E **48**, 1390, (1993). H. Mosshammer, Nucl. Inst. Methods A **323**, 553, (1992). H. Mosshammer, Phys. Rev. E **48**, 2140, (1993).

[2] J. M. Byrd, G. Stupakov, *Proc. of the 1998 Conf. on Quantum Aspects of Beam Physics*, ed. P. Chen (1998).

[3] T. Kasuga, H. Yonehara, M. Hasumoto, and T. Kinoshita, *Jpn. J. Appl. Phys.* **28** (1989) 541. M. Tobiyama, A. Higuchi, T. Mitsuhashi, T. Kasuga, S. Sakanaka, *Proc. of the 1995 Part. Accel. Conf.* (1995) 3300.

[4] W. Decking, D. Robin, Proc. of the 16th Advanced Beam Dynamics Workshop, Arcidosso, (1998).

[5] M. Ellison, et. al., Phys. Rev. Lett. **70**, 591, (1993). H. Huang, et. al., Phys. Rev. E **48**, 4678, 1993. G. Tsironis, S. Peggs, T. Chen, 1990 EPAC, p1753. J. Ellison, H.-J. Shih, M. Kummer, Phys. Rev. E **49**, 2484, (1994). D. Li et al., Phys. Rev. E **48**, 1638, (1993). D. Li et al., Nucl. Instr. Methods A 361, p. 205–223 (1995).

[6] J. M. Byrd, W.H. Cheng, F. Zimmermann, Phys. Rev. E **57**, 4706, (1998).